OPEN ACCESS Freely available online

PLOS ONE

Three-Dimensional Mixed Convection Flow of Viscoelastic Fluid with Thermal Radiation and Convective Conditions

Tasawar Hayat[1,2], Muhammad Bilal Ashraf[1]*, Hamed H. Alsulami[2], Muhammad Shahab Alhuthali[2]

1 Department of Mathematics, Quaid-i-Azam University, Islamabad, Pakistan, **2** Nonlinear Analysis and Applied Mathematics (NAAM) Research Group, Faculty of Science, King Abdulaziz University, Jeddah, Saudi Arabia

Abstract

The objective of present research is to examine the thermal radiation effect in three-dimensional mixed convection flow of viscoelastic fluid. The boundary layer analysis has been discussed for flow by an exponentially stretching surface with convective conditions. The resulting partial differential equations are reduced into a system of nonlinear ordinary differential equations using appropriate transformations. The series solutions are developed through a modern technique known as the homotopy analysis method. The convergent expressions of velocity components and temperature are derived. The solutions obtained are dependent on seven sundry parameters including the viscoelastic parameter, mixed convection parameter, ratio parameter, temperature exponent, Prandtl number, Biot number and radiation parameter. A systematic study is performed to analyze the impacts of these influential parameters on the velocity and temperature, the skin friction coefficients and the local Nusselt number. It is observed that mixed convection parameter in momentum and thermal boundary layers has opposite role. Thermal boundary layer is found to decrease when ratio parameter, Prandtl number and temperature exponent are increased. Local Nusselt number is increasing function of viscoelastic parameter and Biot number. Radiation parameter on the Nusselt number has opposite effects when compared with viscoelastic parameter.

Citation: Hayat T, Ashraf MB, Alsulami HH, Alhuthali MS (2014) Three-Dimensional Mixed Convection Flow of Viscoelastic Fluid with Thermal Radiation and Convective Conditions. PLoS ONE 9(3): e90038. doi:10.1371/journal.pone.0090038

Editor: Enrique Hernandez-Lemus, National Institute of Genomic Medicine, Mexico

Received August 2, 2013; **Accepted** January 30, 2014; **Published** March 7, 2014

Funding: This paper was funded by the Deanship of Scientific Research (DSR), King Abdulaziz University, Jeddah, under grant number 26-130-35 Hi Ci. The authors, therefore, acknowledge with thanks DSR technical and financial support. The funder had no role in the study design, data collection and analysis, decision to publish, or preparation of the manuscript.

Competing Interests: The authors have declared that no competing interests exist.

* E-mail: bilalashraf_qau@yahoo.com

Introduction

Analysis of non-Newtonian fluids is an active area of research for the last few years. Such fluids represent many industrially important fluids including certain oils, shampoos, paints, blood at low shear rate, cosmetic products, polymers, body fluids, colloidal fluids, suspension fluids, pasta, ice cream, ice, mud, dough floor etc. In many fields such as food industry, drilling operations and bioengineering, the fluids, either synthetic or natural, are mixtures of different stuffs such as water, particle, oils, red cells and other long chain molecules. Such combination imparts strong rheological properties to the resulting liquids. The dynamic viscosity in non-Newtonian materials varies non-linearly with the shear rate; elasticity is felt through elongational effects and time-dependent effects. The fluids in these situations have been treated as viscoelastic fluids. Further, all the non-Newtonian fluids in nature cannot be predicted by single constitutive equation. Hence all the contributors in the field are using different models of non-Newtonian fluids in their theoretical and experimental studies (see [1-11] and several refs. therein). The boundary layer flows of non-Newtonian fluids in the presence of heat transfer have special importance because of practical engineering applications such as food processing and oil recovery. Especially the stretching flows in this direction are prominent in polymer extrusion, glass fiber and paper production, plastic films, metal extrusion and many others. After the pioneering works of Sakiadis [12] and Crane [13], numerous works have been presented for two-dimensional boundary layer flow of viscous and non-Newtonian fluids over a surface subject to linear and power law stretching velocities (see some recent studies [14-21]). It has been noted by Gupta and Gupta [22] that stretching mechanism in all realistic situations is not linear. For instance the stretching is not linear in plastic and paper production industries. Besides these the flow and heat transfer by an exponentially stretching surface has been studied by Magyari and Keller [23]. In this attempt the two-dimensional flow of an incompressible viscous fluid is considered. The solutions of laminar boundary layer equations describing heat and flow in a quiescent fluid driven by an exponentially permeable stretching surface are numerically analyzed by Elbashbashy [24]. Al- Odat et al. [25] numerically discussed the thermal boundary layer on an exponentially stretching surface with an exponential temperature distribution. Here magnetohydrodynamic flow is addressed. Nadeem and Lee [26] presented the steady boundary layer flow of nanofluid over an exponential stretching surface. Sajid and Hayat [27] examined the thermal radiation effect in the boundary layer flow and heat transfer of a viscous fluid. The flow is caused by an exponentially stretching sheet. The thermal radiation effect in steady hydromagnetic mixed convection flow of viscous incompressible fluid past an exponentially stretching sheet is examined by El-Aziz and Nabil [28]. Pal [29] carried out an

analysis to describe mixed convection heat transfer in the boundary layer flow on an exponentially stretching continuous surface with an exponential temperature. Here analysis is given in the presence of magnetic field, viscous dissipation and internal heat generation/absorption. Khan and Sanajayand [30] investigated the heat and mass transfer effects of viscoelastic boundary layer flow over an exponentially stretching sheet in presence of viscous dissipation and chemical reaction. Bhattacharyya [31] numerically investigated the heat transfer boundary layer flow over an exponentially shrinking sheet. Shooting method is implemented here. Recently, Mukhopadhyay et al. [32] dealt with the boundary layer flow and heat transfer of a non-Newtonian fluid over an exponentially stretching permeable surface. Mustafa et al. [33] studied the boundary layer flow of nanofluid over an exponentially stretching sheet with convective boundary conditions. Flow and heat transfer for three-dimensional viscous flow over an exponentially stretching surface is discussed by Liu et al. [34]. Bhattacharyya et al. [35] studied the effects of thermal radiation in the flow of micropolar fluid past a porous shrinking sheet with heat transfer. The transient free convection interaction with thermal radiation of an absorbing emitting fluid along moving vertical permeable plate is discussed by Makinde [36]. Hayat et al. [37] considered a two-dimensional mixed convection boundary layer MHD stagnation point flow through a porous medium bounded by a stretching vertical plate with thermal radiation.

Literature survey indicates that the published studies about three-dimensional flow by an exponentially stretching surface are still scarce. To our knowledge, there is only one recent study by Liu et al. [34] which describes the three-dimensional boundary layer flow of a viscous fluid over an exponentially stretching surface. Thus motivation of present research is to venture further in the regime of three-dimensional mixed convection flow of viscoelastic fluid over an exponentially stretching surface with thermal radiation. The surface possess the convective type heat condition. No doubt the thermal radiation effects are significant in many environmental and scientific developments, for instance, in aeronautics, fire research, heating and cooling of channels, etc. It is found that radiative transport is often comparable and hence associated with that of convective heat transfer in several real-world applications. Therefore it is of great worth to the researchers to study combined radiative and convective flow and heat transfer aspects. Moreover, the skin friction coefficients for three-dimensional viscoelastic fluid have been computed which has not yet been available in the literature. This paper is structured into the following fashion. Section two consists of mathematical formulation and definitions of physical quantities of interest. Convergent series solutions of the involved nonlinear systems are developed in section three. The solutions in this section are developed by homotopy analysis method (HAM) [38-45]. Section four comprises discussion with respect to seven pertinent parameters involved in the solutions of velocity components and temperature. Section five syntheses the main observations.

Mathematical Modelling

We consider three dimensional mixed convection boundary layer flow of second grade fluid passing an exponentially stretching surface. The surface coincides with the plane $z=0$ and the flow is confined in the region $z>0$. The surface also possess the convective boundary condition. Influence of thermal radiation through Rosseland's approximation is taken into account. Flow configuration is given below in Fig. 1.

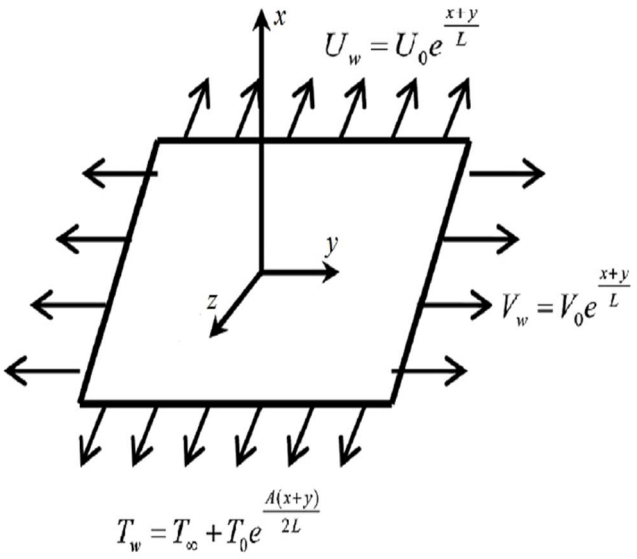

Figure 1. Geometry of Problem.
doi:10.1371/journal.pone.0090038.g001

The governing boundary layer equations for steady three-dimensional flow of viscoelastic fluid can be put into the forms (see Nazar and Latip [11]):

$$\frac{\partial u}{\partial x}+\frac{\partial v}{\partial y}+\frac{\partial w}{\partial z}=0, \tag{1}$$

$$u\frac{\partial u}{\partial x}+v\frac{\partial u}{\partial y}+w\frac{\partial u}{\partial z}=v\frac{\partial^2 u}{\partial z^2} + \frac{k_0}{\rho}\left(u\frac{\partial^3 u}{\partial x\partial z^2}+w\frac{\partial^3 u}{\partial z^3}-\left(\begin{array}{c}\frac{\partial u}{\partial x}\frac{\partial^2 u}{\partial z^2}+\frac{\partial u}{\partial z}\frac{\partial^2 w}{\partial z^2}\\ +2\frac{\partial u}{\partial z}\frac{\partial^2 u}{\partial x\partial z}+2\frac{\partial w}{\partial z}\frac{\partial^2 u}{\partial z^2}\end{array}\right)\right) + g\beta_T(T-T_\infty), \tag{2}$$

$$u\frac{\partial v}{\partial x}+v\frac{\partial v}{\partial y}+w\frac{\partial v}{\partial z}=v\frac{\partial^2 v}{\partial z^2}+ \frac{k_0}{\rho}\left(v\frac{\partial^3 v}{\partial y\partial z^2}+w\frac{\partial^3 v}{\partial z^3}-\left(\begin{array}{c}\frac{\partial v}{\partial y}\frac{\partial^2 v}{\partial z^2}+\frac{\partial v}{\partial z}\frac{\partial^2 w}{\partial z^2}\\ +2\frac{\partial v}{\partial z}\frac{\partial^2 v}{\partial y\partial z}+2\frac{\partial w}{\partial z}\frac{\partial^2 v}{\partial z^2}\end{array}\right)\right), \tag{3}$$

$$u\frac{\partial T}{\partial x}+v\frac{\partial T}{\partial y}+w\frac{\partial T}{\partial z}=\frac{k}{\rho c_p}\frac{\partial^2 T}{\partial z^2}-\frac{1}{\rho c_p}\frac{\partial q_r}{\partial z}, \tag{4}$$

where u, v and w are the velocity components in the $x-$, $y-$ and $z-$ directions respectively, k_0 is the material fluid parameter, μ is the dynamic viscosity, $\nu=(\mu/\rho)$ is the kinematic viscosity, T is the fluid temperature, ρ is the fluid density, g is the gravitational acceleration, β_T is thermal expansion coefficient of temperature, c_p is the specific heat, k is the thermal conductivity and q_r the radiative heat flux. Note that w-momentum equation vanishes by applying boundary layer assumptions (see Schlichting [46]).

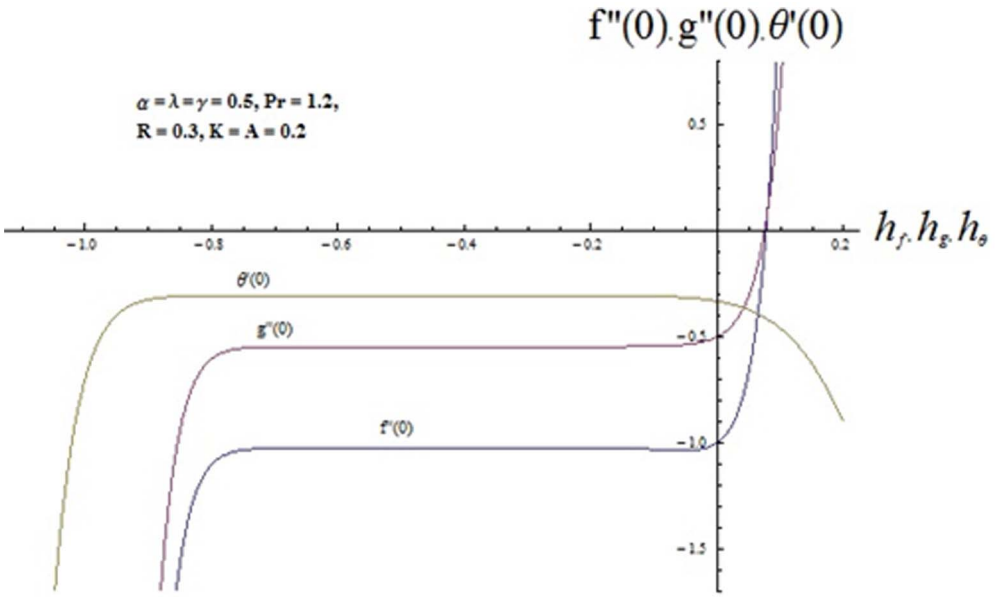

Figure 2. $\hbar-$curvesforthefunctions$f(\eta)$, $g(\eta)$and$\theta(\eta)$.
doi:10.1371/journal.pone.0090038.g002

By using the Rosseland approximation, the radiative heat flux q_r is given by

$$q_r = -\frac{4\sigma_s}{3k_e}\frac{\partial T^4}{\partial z} \tag{5}$$

Where $\sigma_s$is the Stefan-Boltzmann constant and k_e the mean absorption coefficient. By using the Rosseland approximation, the present analysis is limited to optically thick fluids. If the temperature differences are sufficiently small then Eq. (5) can be linearized by expanding T^4 into the Taylor series about T_∞, which after neglecting higher order terms takes the form:

$$T^4 = 4T_\infty^3 T - 3T_\infty^4. \tag{6}$$

By using Eqs. (5) and (6), Eq. (4) reduces to

$$u\frac{\partial T}{\partial x} + v\frac{\partial T}{\partial y} + w\frac{\partial T}{\partial z} = \frac{k}{\rho c_p}\frac{\partial^2 T}{\partial z^2} - \frac{16\sigma_s T_\infty^3}{3k_e\rho c_p}\frac{\partial^2 T}{\partial z^2}, \tag{7}$$

The boundary conditions can be expressed as

$$u = U_w, v = V_w, w = 0, -k\frac{\partial T}{\partial z} = h(T_f - T), \text{at} z = 0,$$

$$u \to 0, v \to 0, T \to T_\infty \text{as} z \to \infty, \tag{8}$$

where subscript w corresponds to the wall condition, $k$is the thermal conductivity, T_f is the hot fluid temperature, $h$is the heat transfer coefficient and $T_\infty$is the free stream temperature.

The velocities and temperature are taken in the following forms:

$$U_w = U_0 e^{\frac{x+y}{L}}, V_w = V_0 e^{\frac{x+y}{L}}, T_w = T_f = T_\infty + T_0 e^{\frac{A(x+y)}{2L}} \tag{9}$$

in which U_0, V_0 are the constants, L is the reference length and $A$is the temperature exponent.

The mathematical analysis of the problem is simplified by using the transformations (Liu et al. [34]):

Table 1. Convergence of series solutions for different order of approximations when $K = 0.1$, $A = 0.2$, $\Pr = 1.2$, $\alpha = 0.2$, $h_f = -0.5, h_g = -0.6$ and $h_0 = -0.7$.

Order of aproximations	1	5	10	15	20	25
-f′′(0)	1.06111	1.02482	1.02609	1.02623	1.02618	1.02618
-g′′ (0)	0.544444	0.548057	0.548092	0.548043	0.548053	0.548053
-θ′ (0)	0.317778	0.305581	0.305729	0.305744	0.305738	0.305738

doi:10.1371/journal.pone.0090038.t001

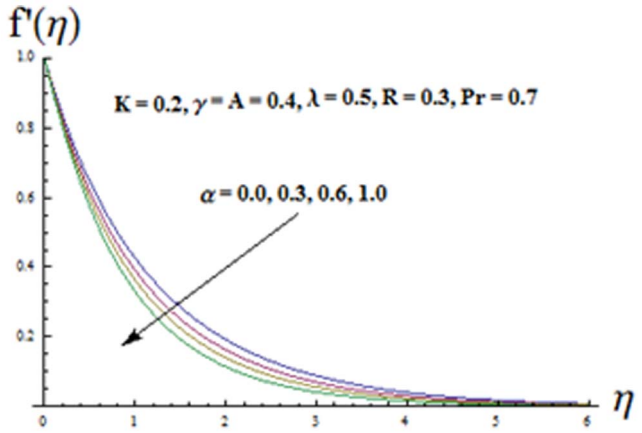

Figure 3. Influence of α on the velocity $f'(\eta)$
doi:10.1371/journal.pone.0090038.g003

$$u = U_0 e^{\frac{x+y}{L}} f'(\eta),\ v = U_0 e^{\frac{x+y}{L}} g'(\eta),$$
$$w = -\left(\frac{\nu U_0}{2L}\right)^{1/2} (f + \eta f' + g + \eta g'), \tag{10}$$
$$T = T_\infty + T_0 e^{\frac{A(x+y)}{2L}} \theta(\eta),\ \eta = \left(\frac{U_0}{2\nu L}\right)^{1/2} e^{\frac{x+y}{2L}} z.$$

Incompressibility condition is now clearly satisfied whereas Eqs. (2)–(7) give

$$f''' + (f+g)f'' - 2(f'+g')f' + K\begin{pmatrix} 6f'''f' + (3g'' - 3f'' + \eta g''')f'' \\ +(4g' + 2\eta g'')f''' - (f + g + \eta g')f'''' \end{pmatrix} + 2\lambda\theta = 0, \tag{11}$$

$$g''' + (f+g)g'' - 2(f'+g')g' + K\begin{pmatrix} 6g'''g' + (3f'' - 3g'' + \eta f''')g'' \\ +(4f' + 2\eta f'')g''' - (f + g + \eta f')g'''' \end{pmatrix} = 0, \tag{12}$$

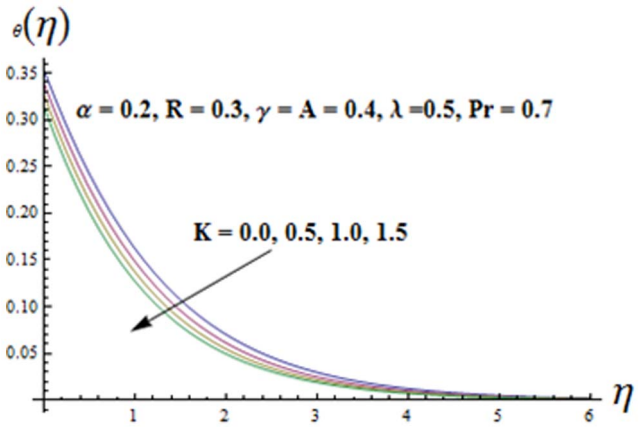

Figure 4. Influence of K on the velocity $f'(\eta)$.
doi:10.1371/journal.pone.0090038.g004

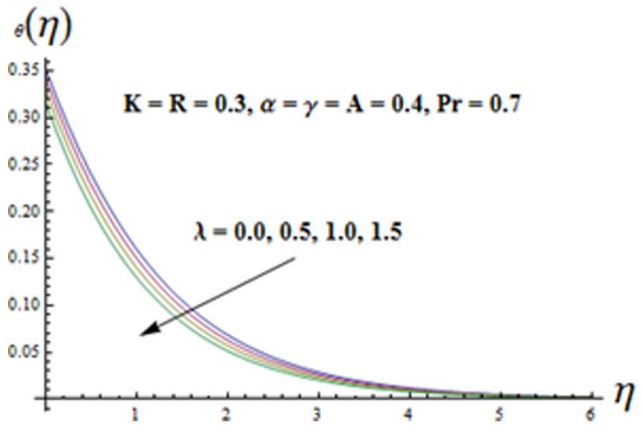

Figure 5. Influence of λ on the velocity $f'(\eta)$.
doi:10.1371/journal.pone.0090038.g005

$$(1 + \frac{4}{3}R)\theta'' + \Pr(f+g)\theta' - \Pr A(f'+g')\theta = 0, \tag{13}$$

$$f = 0, g = 0, f' = 1, g' = \alpha, \theta' = -\gamma(1 - \theta(0)) \text{ at } \eta = 0, \tag{14}$$

$$f' \to 0, g' \to 0, \theta \to 0 \text{ as } \eta \to \infty \tag{15}$$

in which K is the viscoelastic parameter, α is the ratio parameter, Pris the Prandtl number, $Gr_x$is the local Grashof number, $R$is the radiation parameter, $A$is the temperature exponent, γ is the Biot number, Re_x is the local Reynold number, λ is the mixed convection parameter and prime denotes the differentiation with respect to η. These can be defined as

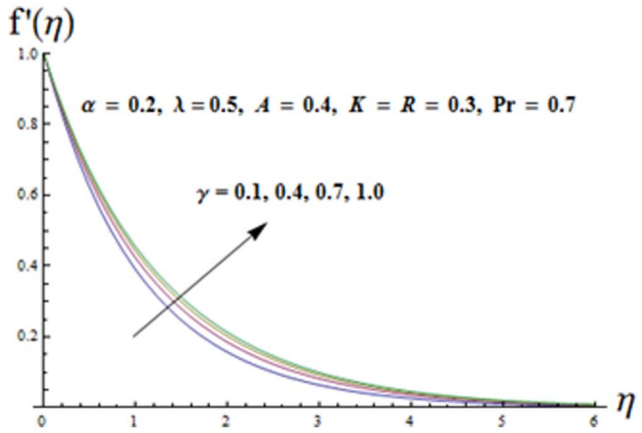

Figure 6. Influence of γ on the velocity $f'(\eta)$.
doi:10.1371/journal.pone.0090038.g006

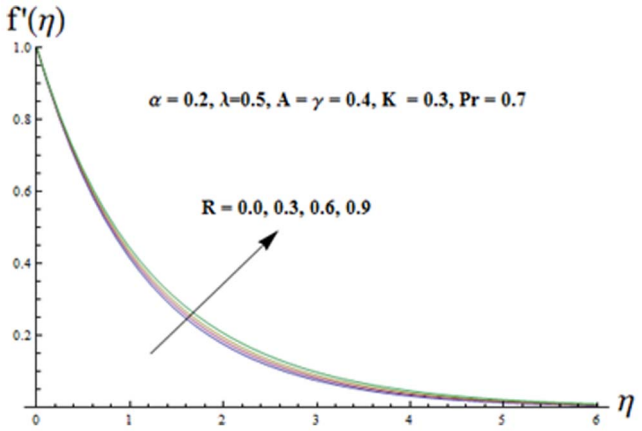

Figure 7. Influence of R on the velocity $f'(\eta)$.
doi:10.1371/journal.pone.0090038.g007

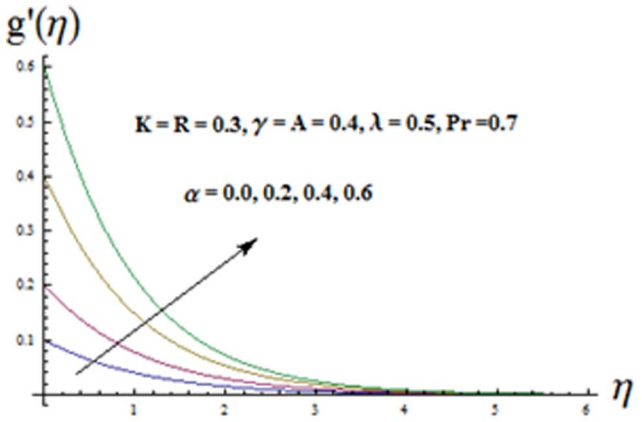

Figure 8. Influence of α on the velocity $g'(\eta)$.
doi:10.1371/journal.pone.0090038.g008

$$K=\frac{k_0U_w}{2\mu L},\ \alpha=\frac{V_0}{U_0},\ \mathrm{Pr}=\frac{\mu c_p}{k},\ R=\left(\frac{4\sigma^* T_\infty^3}{k_e k}\right),\ \gamma=\frac{h}{k}\sqrt{\frac{2\nu L}{U_w}},$$
$$\mathrm{Re}_x=\frac{U_0 L}{\nu}e^{\frac{x+y}{L}},\ \lambda=\frac{Gr_x}{Re_x^2},\ Gr_x=\frac{g\beta_T(T_f-T_\infty)x^3}{\upsilon^2}. \quad (16)$$

The skin-friction coefficients in the x and y directions are given by

$$C_{fx}=\frac{\tau_{wx}}{1/2\rho U_w^2},$$
$$C_{fy}=\frac{\tau_{wy}}{1/2\rho U_w^2}, \quad (17)$$

where

$$\tau_{wx}|_{z=0}=\left(\mu\frac{\partial u}{\partial z}+k_0\left[\begin{array}{l}u\frac{\partial^2 u}{\partial x\partial z}+v\frac{\partial^2 u}{\partial y\partial z}+w\frac{\partial^2 u}{\partial z^2}+\frac{\partial u}{\partial z}\frac{\partial u}{\partial x}\\ +\frac{\partial v}{\partial z}\frac{\partial v}{\partial x}+2\frac{\partial w}{\partial z}\frac{\partial w}{\partial x}-\frac{\partial w}{\partial z}\frac{\partial u}{\partial z}\end{array}\right]\right)_{z=0},$$
$$\tau_{wy}|_{z=0}=\left(\mu\frac{\partial v}{\partial z}+k_0\left[\begin{array}{l}u\frac{\partial^2 v}{\partial x\partial z}+v\frac{\partial^2 v}{\partial y\partial z}+w\frac{\partial^2 v}{\partial z^2}+\frac{\partial u}{\partial z}\frac{\partial u}{\partial y}\\ +\frac{\partial v}{\partial z}\frac{\partial v}{\partial y}+2\frac{\partial w}{\partial z}\frac{\partial w}{\partial y}-\frac{\partial w}{\partial z}\frac{\partial v}{\partial z}\end{array}\right]\right)_{z=0} \quad (18)$$

By using Eq. (18) in Eq. (17) the non-dimensional forms of skin friction coefficients are as follows:

$$C_{fx}=\left(\frac{Re}{2}\right)^{-1/2}[f''+K(-(f+g)f'''+5(f'+g')f''+2f'f''+2g'g'')]_{\eta=0}, \quad (19)$$

$$C_{fy}=\left(\frac{Re}{2}\right)^{-1/2}[g''+K(-(f+g)g'''+5(f'+g')g''+2f'f''+2g'g'')]_{\eta=0}. \quad (20)$$

Further the local Nusselt number has the form

$$Nu=\frac{-\left(\frac{16\sigma^* T_\infty^3}{3k^*}+k\right)\frac{\partial T}{\partial z}}{k(T_w-T_\infty)/x}=-\frac{x}{L}\left(\frac{Re}{2}\right)^{1/2}\left(1+\frac{4}{3}R\right)\theta'(0). \quad (21)$$

Series Solutions

The initial guesses and auxiliary linear operators in the desired HAM solutions are

$$f_0(\eta)=(1-e^{-\eta}),\ g_0(\eta)=\alpha(1-e^{-\eta}),\ \theta_0(\eta)=\exp(-\eta) \quad (22)$$

$$L_f=f'''-f',\ L_g=g'''-g',\ L_\theta=\theta''-\theta \quad (23)$$

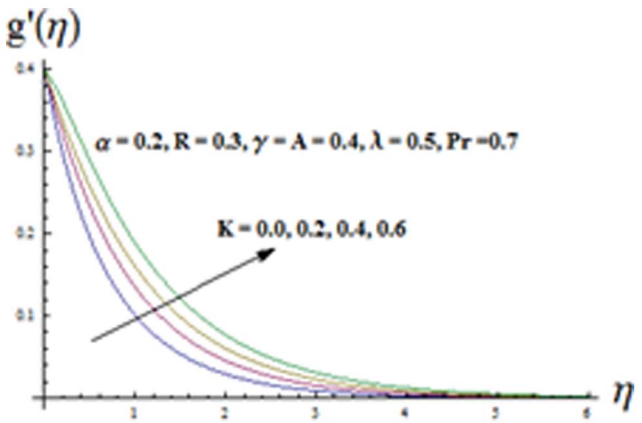

Figure 9. Influence of K on the velocity $g'(\eta)$.
doi:10.1371/journal.pone.0090038.g009

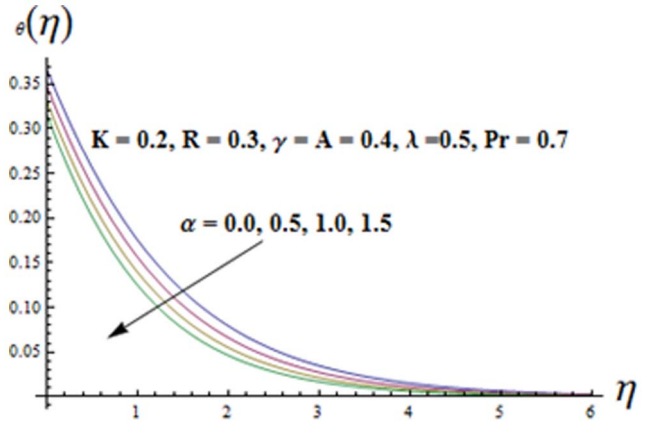

Figure 10. Influence of α on the temperature $\theta(\eta)$.
doi:10.1371/journal.pone.0090038.g010

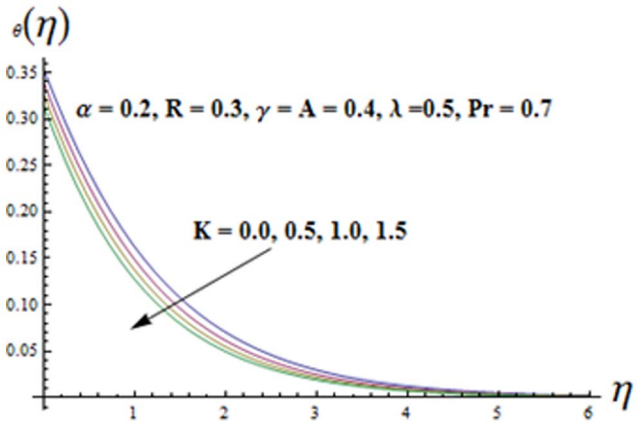

Figure 11. Influence of K on the temperature $\theta(\eta)$.
doi:10.1371/journal.pone.0090038.g011

subject to the properties

$$L_f(C_1+C_2e^{\eta}+C_3e^{-\eta})=0,\ L_g(C_4+C_5e^{\eta}+C_6e^{-\eta})=0,\\ L_\theta(C_7e^{\eta}+C_8e^{-\eta})=0 \tag{24}$$

in which C_i $(i=1-8)$ are the arbitrary constants, L_f, L_g and L_θ are the linear operators and $f_0(\eta), g_0(\eta)$ and $\theta_0(\eta)$ are the initial guesses.

Following the idea in ref. [38] the zeroth order deformation problems are

$$(1-p)L_f\left[\hat{f}(\eta;\,p)-f_0(\eta)\right]=p\hbar_f\mathbf{N}_f\left[\hat{f}(\eta;\,p),\hat{g}(\eta;\,p)\right], \tag{25}$$

$$(1-p)L_g[\hat{g}(\eta;\,p)-g_0(\eta)]=p\hbar_g\mathbf{N}_g\left[\hat{f}(\eta;\,p),\hat{g}(\eta;\,p)\right], \tag{26}$$

$$(1-p)L_\theta\left[\hat{\theta}(\eta;\,p)-\theta_0(\eta)\right]=p\hbar_\theta\mathbf{N}_\theta\left[\hat{f}(\eta;\,p),\hat{g}(\eta;\,p),\hat{\theta}(\eta,p)\right], \tag{27}$$

$$\hat{f}(0;\,p)=0,\hat{f}'(0;\,p)=1,\hat{f}'(\infty;\,p)=0,\hat{g}(0;\,p)=0,\\ \hat{g}'(0;\,p)=\alpha,\hat{g}'(\infty;\,p)=0,\hat{\theta}'(0,p)=-\gamma[1-\theta(0,p)], \\ \hat{\theta}(\infty,p)=0, \tag{28}$$

For $p=0$ and $p=1$ one has

$$\hat{f}(\eta;\,0)=f_0(\eta),\hat{g}(\eta;\,0)=g_0(\eta),\\ \hat{\theta}(\eta,0)=\theta_0(\eta),\text{and}\hat{f}(\eta;\,1)=f(\eta), \\ \hat{g}(\eta;\,1)=g(\eta),\hat{\theta}(\eta,1)=\theta(\eta). \tag{29}$$

Note that when p increases from 0 to 1 then $f(\eta,p)$, $g(\eta,p)$ and $\theta(\eta,p)$ vary from $f_0(\eta)$, $g_0(\eta)$ and $\theta_0(\eta)$ to $f(\eta)$, $g(\eta)$and$\theta(\eta)$. So as the embedding parameter $p\in[0,1]$ increases from 0 to 1, the solutions $\hat{f}(\eta;\,p),\hat{g}(\eta;\,p)$ and $\hat{\theta}(\eta;\,p)$ of the zeroth order deformation equations deform from the initial guesses $f_0(\eta), g_0(\eta)$ and $\theta_0(\eta)$to the exact solutions$f(\eta), g(\eta)$and $\theta(\eta)$of the original nonlinear differential equations. Such kind of continuous variation is called deformation in topology and that is why the Eqs. (26-28) are called the zeroth order deformation equations. The values of the nonlinear operators are given below:

$$\begin{aligned}N_f[\hat{f}(\eta,p),\hat{g}(\eta,p)]=&\frac{\partial^3\hat{f}(\eta,p)}{\partial\eta^3}-2\left(\frac{\partial\hat{f}(\eta,p)}{\partial\eta}+\frac{\partial\hat{g}(\eta,p)}{\partial\eta}\right)\frac{\partial\hat{f}(\eta,p)}{\partial\eta}\\&+\left(\hat{f}(\eta,p)+\hat{g}(\eta,p)\right)\frac{\partial^2\hat{f}(\eta,p)}{\partial\eta^2}\\&+K\left(\begin{array}{c}6\frac{\partial\hat{f}(\eta,p)}{\partial\eta}\frac{\partial^3\hat{f}(\eta,p)}{\partial\eta^3}+\left(3\frac{\partial^2\hat{g}(\eta,p)}{\partial\eta^2}-3\frac{\partial^2\hat{f}(\eta,p)}{\partial\eta^2}+\eta\frac{\partial^3\hat{g}(\eta,p)}{\partial\eta^3}\right)\\ \frac{\partial^2\hat{f}(\eta,p)}{\partial\eta^2}+\left(4\frac{\partial\hat{g}(\eta,p)}{\partial\eta}+2\eta\frac{\partial^2\hat{g}(\eta,p)}{\partial\eta^2}\right)\frac{\partial^3\hat{f}(\eta,p)}{\partial\eta^3}\\ -\left(\hat{f}(\eta,p)+\hat{g}(\eta,p)+\eta\frac{\partial\hat{g}(\eta,p)}{\partial\eta}\right)\frac{\partial^4\hat{f}(\eta,p)}{\partial\eta^4}\end{array}\right)\\&+2\lambda\hat{\theta}(\eta,p),\end{aligned} \tag{30}$$

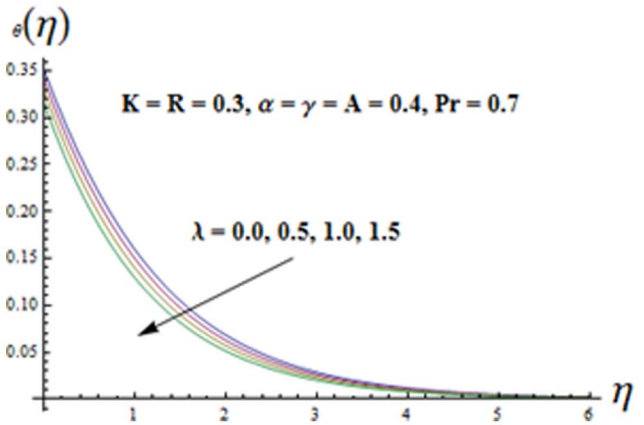

Figure 12. Influence of λ on the temperature $\theta(\eta)$.
doi:10.1371/journal.pone.0090038.g012

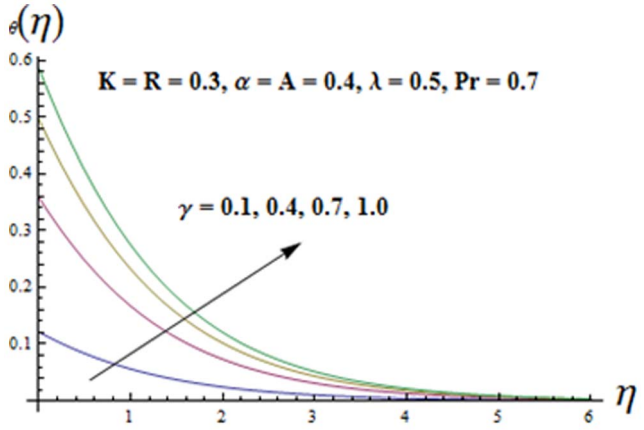

Figure 13. Influence of γ on the temperature $\theta(\eta)$.
doi:10.1371/journal.pone.0090038.g013

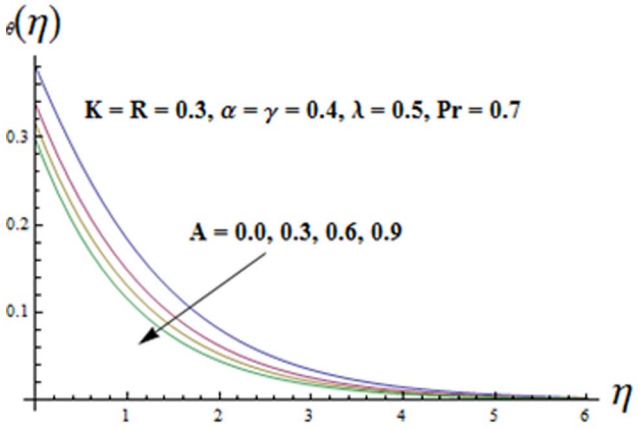

Figure 14. Influence of A on the temperature $\theta(\eta)$.
doi:10.1371/journal.pone.0090038.g014

$$N_g[\hat{g}(\eta,p),\hat{f}(\eta,p)] = \frac{\partial^3 \hat{g}(\eta,p)}{\partial \eta^3} - 2\left(\begin{array}{c}\frac{\partial \hat{f}(\eta,p)}{\partial \eta}\\ +\frac{\partial \hat{g}(\eta,p)}{\partial \eta}\end{array}\right)\frac{\partial \hat{g}(\eta,p)}{\partial \eta} + \left(\begin{array}{c}\hat{f}(\eta,p)\\ +\hat{g}(\eta,p)\end{array}\right)\frac{\partial^2 \hat{g}(\eta,p)}{\partial \eta^2} + K\left(\begin{array}{c} 6\frac{\partial \hat{g}(\eta,p)}{\partial \eta}\frac{\partial^3 \hat{g}(\eta,p)}{\partial \eta^3} + \left(3\frac{\partial^2 \hat{f}(\eta,p)}{\partial \eta^2} - 3\frac{\partial^2 \hat{g}(\eta,p)}{\partial \eta^2} + \eta\frac{\partial^3 \hat{f}(\eta,p)}{\partial \eta^3}\right) \\ \frac{\partial^2 \hat{g}(\eta,p)}{\partial \eta^2} + \left(4\frac{\partial \hat{f}(\eta,p)}{\partial \eta} + 2\eta\frac{\partial^2 \hat{f}(\eta,p)}{\partial \eta^2}\right)\frac{\partial^3 \hat{g}(\eta,p)}{\partial \eta^3} \\ -\left(\hat{f}(\eta,p)+\hat{g}(\eta,p)+\eta\frac{\partial \hat{f}(\eta,p)}{\partial \eta}\right)\frac{\partial^4 \hat{g}(\eta,p)}{\partial \eta^4}\end{array}\right), \quad (31)$$

$$N_\theta[\hat{\theta}(\eta,p),\hat{f}(\eta,p),\hat{g}(\eta,p)] = (1+\frac{4}{3}R)\frac{\partial^2 \hat{\theta}(\eta,p)}{\partial \eta^2} + \Pr\left(\hat{f}(\eta,p)+\hat{g}(\eta,p)\right)\frac{\partial \hat{\theta}(\eta,p)}{\partial \eta} - \Pr A\left(\frac{\partial \hat{f}(\eta,p)}{\partial \eta}+\frac{\partial \hat{g}(\eta,p)}{\partial \eta}\right)\hat{\theta}(\eta,p). \quad (32)$$

Here $\hbar_f$,$\hbar_g$and $\hbar_\theta$ are the non-zero auxiliary parameters and $\mathbf{N}_f$,$\mathbf{N}_g$and $\mathbf{N}_\theta$ the nonlinear operators. Taylor series expansion gives

$$f(\eta,p) = f_0(\eta) + \sum_{m=1}^{\infty} f_m(\eta)p^m, f_m(\eta) = \frac{1}{m!}\frac{\partial^m f(\eta;\, p)}{\partial p^m}\bigg|_{p=0}, \quad (33)$$

$$g(\eta,p) = g_0(\eta) + \sum_{m=1}^{\infty} g_m(\eta)p^m, g_m(\eta) = \frac{1}{m!}\frac{\partial^m g(\eta;\, p)}{\partial p^m}\bigg|_{p=0}, \quad (34)$$

$$\theta(\eta,p) = \theta_0(\eta) \sum_{m=1}^{\infty} \theta_m(\eta)p^m, \theta_m(\eta) = \frac{1}{m!}\frac{\partial^m \theta(\eta;\, p)}{\partial p^m}\bigg|_{p=0}, \quad (35)$$

where the convergence of above series strongly depends upon $\hbar_f$,$\hbar_g$and $\hbar_\theta$. Considering that $\hbar_f$, $\hbar_g$ and $\hbar_\theta$are chosen in such a manner that Eqs. (33)-(35) converge at $p=1$ then

$$f(\eta) = f_0(\eta) + \sum_{m=1}^{\infty} f_m(\eta), \quad (36)$$

$$g(\eta) = g_0(\eta) + \sum_{m=1}^{\infty} g_m(\eta), \quad (37)$$

$$\theta(\eta) = \theta_0(\eta) + \sum_{m=1}^{\infty} \theta_m(\eta). \quad (38)$$

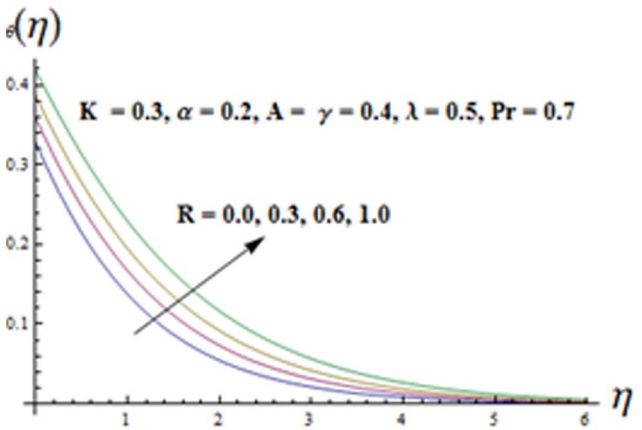

Figure 15. Influence of R on the temperature $\theta(\eta)$.
doi:10.1371/journal.pone.0090038.g015

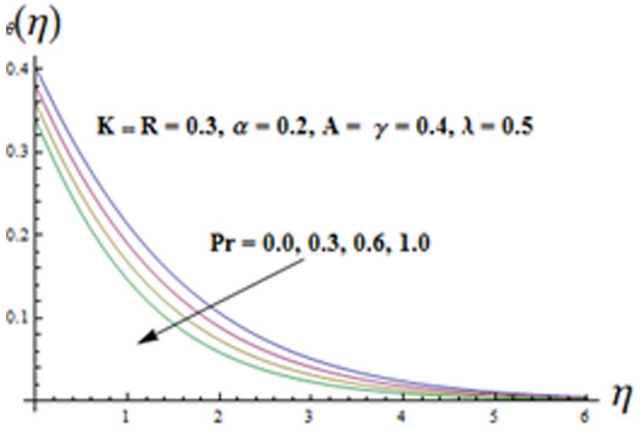

Figure16. Influence of Pr **on the temperature** $\theta(\eta)$
doi:10.1371/journal.pone.0090038.g016

The corresponding problems at mth order deformations satisfy

$$L_f[f_m(\eta)-\chi_m f_{m-1}(\eta)]=\hbar_f \mathbf{R}_f^m(\eta), \tag{39}$$

$$L_g[g_m(\eta)-\chi_m g_{m-1}(\eta)]=\hbar_g \mathbf{R}_g^m(\eta), \tag{40}$$

$$L_\theta[\theta_m(\eta)-\chi_m \theta_{m-1}(\eta)]=\hbar_\theta \mathbf{R}_\theta^m(\eta). \tag{41}$$

$$\begin{aligned} &f_m(0)=f_m'(0)=f_m'(\infty)=0, g_m(0)=g_m'(0)=g_m'(\infty)=0,\\ &\theta_m'(0)-\gamma\theta_m(0)=\theta_m(\infty)=0, \end{aligned} \tag{42}$$

$$\begin{aligned} R_f^m(\eta)=&f_{m-1}'''(\eta)-2\sum_{k=0}^{m-1} f_{m-1-k}' f_k'-2\sum_{k=0}^{m-1} g_{m-1-k}' f_k'\\ &+\sum_{k=0}^{m-1}(f_{m-1-k}f_k''+g_{m-1-k}f_k'')\\ &+K\begin{pmatrix} 6\sum_{k=0}^{m-1} f_{m-1-k}' f_k'''+3\sum_{k=0}^{m-1} g_{m-1-k}'' f_k''-3\sum_{k=0}^{m-1} f_{m-1-k}'' f_k''\\ +\sum_{k=0}^{m-1}\eta g_{m-1-k}''' f_k''+4\sum_{k=0}^{m-1} g_{m-1-k}' f_k'''+2\sum_{k=0}^{m-1}\eta g_{m-1-k}'' f_k'''\\ -\sum_{k=0}^{m-1} f_{m-1-k} f_k''''-\sum_{k=0}^{m-1} g_{m-1-k} f_k'''-\sum_{k=0}^{m-1}\eta g_{m-1-k}' f_k'''' \end{pmatrix}\\ &+2\lambda\theta, \end{aligned} \tag{43}$$

$$\begin{aligned} R_g^m(\eta)=&g_{m-1}'''(\eta)-2\sum_{k=0}^{m-1} g_{m-1-k}' g_k'-2\sum_{k=0}^{m-1} g_{m-1-k}' f_k'\\ &+\sum_{k=0}^{m-1}(f_{m-1-k}g_k''+g_{m-1-k}g_k'')\\ &+K\begin{pmatrix} 6\sum_{k=0}^{m-1} g_{m-1-k}' g_k'''+3\sum_{k=0}^{m-1} f_{m-1-k}'' g_k''-3\sum_{k=0}^{m-1} g_{m-1-k}'' g_k''\\ +\sum_{k=0}^{m-1}\eta f_{m-1-k}''' g_k''+4\sum_{k=0}^{m-1} f_{m-1-k}' g_k'''+2\sum_{k=0}^{m-1}\eta f_{m-1-k}'' g_k'''\\ -\sum_{k=0}^{m-1} g_{m-1-k} g_k''''-\sum_{k=0}^{m-1} f_{m-1-k} g_k''''-\sum_{k=0}^{m-1}\eta f_{m-1-k}' g_k'''' \end{pmatrix}, \end{aligned} \tag{44}$$

$$\begin{aligned} R_\theta^m(\eta)=&(1+\frac{4}{3}R)\theta_{m-1}''\\ &+\Pr\sum k=0^{m-1}(\theta_{m-1-k}' f_k+\theta_{m-1-k}' g_k)\\ &-\Pr A\sum_{k=0}^{m-1}(f_{m-1-k}'\theta_k+g_{m-1-k}'\theta_k), \end{aligned} \tag{45}$$

The mth order deformation problems have the solutions

$$f_m(\eta)=f_m^*(\eta)+C_1+C_2e^{\eta}+C_3e^{-\eta}, \tag{46}$$

$$g_m(\eta)=g_m^*(\eta)+C_4+C_5e^{\eta}+C_6e^{-\eta}, \tag{47}$$

$$\theta_m(\eta)=\theta_m^*(\eta)+C_7e^{\eta}+C_8e^{-\eta}, \tag{48}$$

where the special solutions are f_m^*, g_m^* and θ_m^*.

Convergence Analysis

We recall that the series (36-38) contain the auxiliary parameters $\hbar_f$, $\hbar_g$ and $\hbar_\theta$. These parameters are useful to adjust and control the convergence of homotopic solutions. Hence the $\hbar-$ curves are sketched at 15^{th} order of approximations in order to determine the suitable ranges for $\hbar_f$, $\hbar_g$ and $\hbar_\theta$. Fig. 2 denotes that the range of admissible values of $\hbar_f$, $\hbar_g$ and $\hbar_\theta$ are $-0.7\le\hbar_f\le-0.2$, $-0.7\le\hbar_g\le-0.1$ and $-0.8\le\hbar_\theta\le-0.2$. Table 1 shows that the series solutions converge in the whole region of η when $\hbar_f=-0.5$,$\hbar_g=-0.6$ and $\hbar_\theta=-0.7$.

Table 2. Comparative values of $-f''(0)$, $-g''(0)$ and $f(\infty)+g(\infty)$ for different values α when $K_1=\lambda=\gamma=R=0$.

Liu et al. [34]				**Present results**		
α	-f′′′ (0)	-g′′ (0)	f(∞)+g(∞)	-f′′ (0)	-g′′ (0)	f(∞)+g(∞)
0.0	1.28180856	0	0.90564383	1.28181	0	0.90564
0.50	1.56988846	0.78494423	1.10918263	1.56989	0.78494	1.10918
1.00	1.81275105	1.81275105	1.28077378	1.81275	1.81275	1.28077

doi:10.1371/journal.pone.0090038.t002

Table 3. Values of skin friction coefficients for different values of K and α when $\lambda=\gamma=0.5$, R = 0.3, Pr = 1.2 and A = 0.2.

K	α	$-\left(\frac{Re}{2}\right)^{1/2}C_{fx}$	$-\left(\frac{Re}{2}\right)^{1/2}C_{fy}$
0.0	0.5	4.95289	4.37363
0.2		5.16586	3.97055
0.3		5.42622	3.96130
0.3	0.0	3.72170	1.65409
	0.2	4.30247	2.34617
	0.5	5.42622	3.96130

doi:10.1371/journal.pone.0090038.t003

Discussion of Results

The effects of ratio parameter α, viscoelastic parameter K, mixed convection parameter λ, Biot number γ and radiation parameter R on the velocity component $f'(\eta)$ are shown in the Figs. 3-7. It is observed from Fig. 3 that velocity component $f'(\eta)$ and thermal boundary layer thickness are decreasing functions of ratio parameter α. This is due to the fact that with the increase of ratio parameter α, the x-component of velocity coefficient decreases which leads to a decrease in both the momentum boundary layer and velocity component $f'(\eta)$. Fig. 4 illustrates the influence of viscoelastic parameter K on the velocity component $f'(\eta)$. It is clear that both the boundary layer and velocity component $f'(\eta)$ increase when the viscoelastic parameter increases. Influence of mixed convection parameter λ on the velocity component $f'(\eta)$ is analyzed in Fig. 5. Increase in mixed convection parameter λ shows an increase in velocity component $f'(\eta)$. This is due to the fact that the buoyancy forces are much more effective rather than the viscous forces. Effects of Biot number γ and the radiation parameter R on the velocity component $f'(\eta)$ can be predicted from Figs. 6 and 7. These Figs. depict that the influences of γ and R on both the velocity component $f'(\eta)$ and thermal boundary layer thickness are similar i.e. there is increase in these quantities. Figs. 8 and 9 illustrate the variations of ratio parameter α and viscoelastic parameter K on the velocity component $g'(\eta)$. Variation of ratio parameter $\alpha$is analyzed in Fig. 8. Through comparative study with Fig. 3 it is noted that $f'(\eta)$ decreases while $g'(\eta)$ increases when α increases. Physically, when α increases from zero, the lateral surface starts moving in y-direction and thus the velocity component $g'(\eta)$ increases and the velocity component $f'(\eta)$ decreases. Fig. 9 is plotted to see the variation of viscoelastic parameter K on the velocity component $g'(\eta)$. It is found that both the velocity component $g'(\eta)$ and momentum boundary layer thicknesses are increasing functions of K. It is revealed from Figs. 4 and 9 that the effect of K on both the velocities are qualitatively similar. Figs. 10-16 are sketched to see the effects of ratio parameter α, viscoelastic parameter K, the temperature exponent A, Biot number γ, mixed convection parameter λ, Radiation parameter and Prandtl number Pr on the temperature $\theta(\eta)$. Fig. 10 is drawn to see the impact of ratio parameter α on the temperature $\theta(\eta)$. It is noted that the temperature $\theta(\eta)$ and also the thermal boundary layer thickness decrease with increasingα. Variation of the viscoelastic parameter K on the temperature $\theta(\eta)$ is shown in Fig. 11. Here both the temperature and thermal boundary layer thickness are decreasing functions of K. Variation of mixed convection parameter λ is analyzed in Fig.12. It is seen that both the temperature $\theta(\eta)$ and thermal boundary layer thickness are decreasing functions of mixed convection parameter λ. Fig.13 presents the plots for the variation of Biot number γ. Note that $\theta(\eta)$ increases when γ increases. The thermal boundary layer thickness is also increasing function of γ. It is also noted that the fluid temperature is zero when the Biot number vanishes. Influence of temperature exponent A is displayed in Fig. 14. It is found that both the temperature $\theta(\eta)$ and thermal boundary layer thickness decrease when A is increased. Also both the temperature $\theta(\eta)$ and thermal boundary layer thickness are increasing functions of thermal radiation parameter R (see Fig. 15). It is observed that an increase in R has the ability to increase the thermal boundary layer. It is due to the fact that when the thermal radiation parameter increases, the mean absorption coefficient k_e will be decreased which in turn increases the divergence of the radiative heat flux. Hence the rate of radiative heat transfer to the fluid is increased and consequently the fluid temperature increases. Fig. 16 is plotted to see the effects of Pr on $\theta(\eta)$. It is noticed that both the temperature profile and thermal boundary layer thickness are decreasing functions of Pr. In fact when Pr increases then thermal diffusivity decreases. This indicates reduction in energy transfer ability and ultimate it results in the decrease of thermal boundary layer.

Table 1 presents the numerical values of $-f''(0)$, $-g''(0)$ and $-\theta'(0)$ for different order of approximations when $\hbar_f=-0.5$,$\hbar_g=-0.6$ and $\hbar_\theta=-0.7$. It is seen that the values of $-f''(0)$ and $-g''(0)$ converge from 20th order of deformations whereas the values of $-\theta'(0)$ converge from 25th order approximations. Further, it is observed that we have to compute less deformations for the velocities in comparison to temperature for convergent series solutions. Table 2 includes the values for

Table 4. Values of local Nusselt number $-\theta'(0)$ for different values of the parameters K, α, λ, R, A, Pr and γ.

K	λ	α	γ	R	Pr	A	$-\theta'(0)$
0.0	0.5	0.5	0.5	0.3	1.2	0.2	0.297492
0.3							0.308234
0.5							0.311853
0.2	0.0						0.303062
	0.3						0.304775
	0.5						0.305738
0.2	0.5	0.0					0.282007
		0.3					0.297135
		0.5					0.305738
			0.1				0.0885730
			0.3				0.216850
			0.5				0.305738
0.2	0.5	0.5	0.5	0.0			0.329701
				0.3			0.305738
				0.5			0.292750
0.2	0.5	0.5	0.5	0.3	1.0		0.292152
					1.2		0.305738
					1.5		0.321826
0.2	0.5	0.5	0.5	0.3	1.2	0.0	0.288530
						0.2	0.305738
						0.5	0.325492

doi:10.1371/journal.pone.0090038.t004

comparison of existing solutions with the previous available solutions in a limiting case when $K_1=\lambda=\gamma=R=0$ and α varies. This Table presents an excellent agreement with the previous available solutions. Table 3 is computed to see the influences of viscoelastic parameter K and ratio parameter α on skin friction coefficients in the x and y directions. It is noted that K has quite opposite effect on skin friction coefficients while quite similar effect is seen within the increase of ratio parameter α. Table 4 examines the impact of viscoelastic parameter K, mixed convection parameter λ, ratio parameter α, Biot number γ, radiation parameter R, Prandtl number Pr and temperature exponent A on the local Nusselt number (rate of heat transfer at the wall). It is noted that the value of rate of heat transfer increases for larger viscoelastic parameter K, mixed convection parameter λ, ratio parameter α, Biot number γ, Prandtl number Pr and temperature exponent A while it decreases through an increase in radiation parameter R.

Table 2. Comparative values of $-f''(0)$, $-g''(0)$ and $f(\infty)+g(\infty)$ for different values α when $K_1=\lambda=\gamma=R=0$.

Conclusions

Three-dimensional mixed convection flow of viscoelastic fluid over an exponentially stretching surface is analyzed in this study. The analysis is carried out in the presence of thermal radiation subject to convective boundary conditions. The main observations can be summarized as follows:

- Influence of ratio parameter α on the velocities $f'(\eta)$ and $g'(\eta)$ is quite opposite. However the effect of viscoelastic parameter K on the velocities $f'(\eta)$ and $g'(\eta)$ is qualitatively similar.
- Momentum boundary layer thickness increases for $g'(\eta)$ when ratio parameter α is large. Effect of α on $f'(\eta)$ is opposite to that of $g'(\eta)$.
- Velocity component $f'(\eta)$ is increasing function of mixed convection parameter λ. However $\theta(\eta)$ decreases with an increase of mixed convection parameter λ. The impact of Biot number γ and radiation parameter R on $f'(\eta)$ and $\theta(\eta)$ are qualitatively similar.
- Momentum boundary layer is an increasing function of mixed convection parameter λ while thermal boundary layer is decreasing function of mixed convection parameter λ.
- Increase in Prandtl number decreases the temperature $\theta(\eta)$.
- Thermal boundary layer thickness decreases when ratio parameter α, viscoelastic parameter K, mixed convection parameter λ, Prandtl number Pr and temperature exponent A are increased.
- Influence of viscoelastic parameter K on the x and y direction of skin friction coefficients is opposite.
- Both components of skin friction coefficient increase through an increase in ratio parameter α.
- Local Nusselt number is an increasing function of Prandtl number Pr, ratio parameter α, viscoelastic parameter K, mixed convection parameter λ, Biot number γ and temperature exponent A while it decreases for radiation parameter R.

Supporting Information

File S1 Appendix.
(DOCX)

Acknowledgments

We are thankful to the reviewers for the useful comments.

Author Contributions

Conceived and designed the experiments: TH MBA HHA MSA. Performed the experiments: TH MBA HHA MSA. Analyzed the data: TH MBA HHA MSA. Contributed reagents/materials/analysis tools: TH MBA HHA MSA. Wrote the paper: TH MBA HHA MSA.

References

1. Turkyilmazoglu M (2011) Multiple solutions of heat and mass transfer of MHD slip flow for the viscoelastic fluid over a stretching sheet. Int J Thermal Sci50: 2264-2276.
2. Keimanesh M, Rashidi MM, Chamkha AJ, Jafari R (2011) Study of a third grade non-Newtonian fluid flow between two parallel plates using the multi-step differential transform method. Comput Math Appl 62 : 2871–2891.
3. Jamil M, Fetecau C (2010) Helical flows of Maxwell fluid between coaxial cylinders with given shear stresses on the boundary. Nonlinear Analysis: Real World Applications 11: 4302-4311.
4. Jamil M, Fetecau C, Imran M (2011) Unsteady helical flows of Oldroyd-B fluids, Commun. Nonlinear Sci. Numer. Simulat 16 : 1378-1386.
5. Liu J, Qi H (2010) Hysteresis and precondition of the standard viscoelastic solid model. Nonlinear Analysis: Real World Applications 11 :3066-3076.
6. Ellahi R (2013) The effects of MHD and temperature dependent viscosity on the flow of non-Newtonian nanofluid in a pipe: analytical solutions Appl Math Modell37 : 1451–1467.
7. Deger G, Pakdemirli M, Aksoy Y (2011) Symmetry analysis of boundary layer equations of an upper convected Maxwell fluid with MHD flow. Zeitschrift für Naturforschung 66a : 321- 328.
8. Hayat T, Shehzad SA, Alsaedi A (2013) Three-dimensional stretched flow of Jeffrey fluid with variable thermal conductivity and thermal radiation. Appl Math Mech Engl Ed 34 : 823–832.
9. Hayat T, Zaib S, Asghar S, Bhattacharyya K, Shehzad SA (2013) Transient flows of Maxwell fluid with slip conditions. Appl Math Mech 34: 153-166.
10. Hayat T, Afzal S, Hendi AA (2012) Exact solution of electroosmotic flow in generalized Burgers fluid. Appl Math Mech 32: 1119-1126.
11. Nazar R, Latip NA (2009) Numerical investigation of three-dimensional boundary layer flow due to a stretching surface in a viscoelastic fluid. Eur J Sci Res 29: 509-517.
12. Sakidia BC (1961) Boundary layer behavior on continuous solid surfaces. AIChE J 7 : 26-28.
13. Crane LJ (1970) Flow past a stretching plate. ZAMP 21: 645-647.
14. Bhattacharyya K, Uddin US, Layek GC, Malek MA (2010) Effect of chemically reactive solute diffusion on boundary layer flow past a stretching surface with suction or blowing. J. Math Math Sci 25: 41-48.
15. Cortell R (2007) Viscous flow and heat transfer over a nonlinearly stretching sheet Appl Math Comput184: 864-873.
16. Hayat T, Javed T, Abbas Z (2009) MHD flow of a micropolar fluid near a stagnation point towards a non-linear stretching surface. Nonlinear Anal.Real World Appl 10: 1514–1526.
17. Bhattacharyya K (2011) Dual solutions in boundary layer stagnation-point flow and mass transfer with chemical reaction past a stretching/shrinking sheet. Int Commun Heat Mass Transf 38: 917–922.
18. Turkyilmazoglu M, Pop I (2013) Exact analytical solutions for the flow and heat transfer near the stagnation point on a stretching/shrinking sheet in a Jeffrey fluid. Int J Heat Mass Transf 57: 82–88.
19. Mukhopadhyay S (2013) Casson fluid flow and heat transfer over a nonlinearly stretching surface. Chin Phys B, 22: 074701.
20. Abbasbandy S, Ghehsareh HR, Hashim I (2012) An approximate solution of the MHD flow over a non-linearly stretching sheet by rational Chebyshev collocation method. UPB Sci Bull 74.
21. Kandasamy R, Hayat T, Obadiat S (2011) Group theory transformation for Soret and Dufour effects on free convective heat and mass transfer with thermophoresis and chemical reaction over a porous stretching surface in the presence of heat source/sink. Nucl Eng Des 241: 2155–2161.
22. Gupta PS, Gupta AS (1977) Heat and mass transfer on a stretching sheet with suction or blowing Can J Chem Eng55: 744-746.
23. Magyari E, Keller B (1999) Heat and mass transfer in the boundary layers on an exponentially stretching continuous surface. J Phys D: Appl Phys 32: 577–585.
24. Elbashbeshy EMA (2001) Heat transfer over an exponentially stretching continuous surface with suction. Arch Mech 53: 643-651.
25. Al-Odat MQ, Damesh RA, Al-Azab TA (2006) Thermal boundary layer on an exponentially stretching continuous surface in the presence of magntic field. Int J Appl Mech Eng 11 : 289-299.
26. Nadeem S, Lee C (2012) Boundary layer flow of nanofluid over an exponentially stretching surface. Nanoscale Research Lett 7: 94.

27. Sajid M, Hayat T (2008) Influence of thermal radiation on the boundary layer flow due to an exponentially stretching sheet. Int Commun Heat Mass Transfer 35: 347-356.
28. Aziz MAE, Nabil T (2012) Homotopy analysis solution of hydromagnetic mixed convection flow past an exponentially stretching sheet with Hall current. Math Prob Eng 2012: 454023.
29. Pal D (2010) Mixed convection heat transfer in the boundary layers on an exponentially stretching surface with magnetic field. Appl Math Comput 217: 2356–2369.
30. Sanjayanand E, Khan SK (2006) On heat and mass transfer in a viscoelastic boundary layer flow over an exponentially stretching sheet. Int J Thermal Sci 45: 819-828.
31. Bhattacharyya K (2011) Boundary layer flow and heat transfer over an exponentially shrinking sheet. Chin Phys Lett 28: 074701.
32. Mukhopadhyay S, Vajravelu K, Gorder RAV (2013) Casson fluid flow and heat transfer at an exponentially stretching permeable surface. J Appl Mech 80: 054502.
33. Mustafa M, Hayat T, Obaidat S (2013) Boundary layer flow of a nanofluid over an exponentially stretching sheet with convective boundary conditions. Int J Numer Meth Heat Fluid Flow 23: 945-959.
34. Liu IC, Wang HH, Peng YF (2013) Flow and heat transfer for three dimensional flow over an exponentially stretching surface. Chem Eng Comm 200: 253-268.
35. Bhattacharyya K, Mukhopadhyay S, Layek GC, Pop I (2012) Effects of thermal radiation on micropolar fluid flow and heat transfer over a porous shrinking sheet. Int J Heat Mass Transf 55: 4945-4952.
36. Makinde OD (2005) Free convection flow with thermal radiation and mass transfer past a moving vertical porous plate. Int Commun Heat Mass Transf 32: 1411–1419.
37. Hayat T, Abbas Z, Pop I, Asghar S (2010) Effects of radiation and magnetic field on the mixed convection stagnation-point flow over a vertical stretching sheet in a porous medium. Int J Heat Mass Transf 53: 466–474.
38. Liao SJ (2003) Beyond perturbation: introduction to the homotopy analysis method. Chapman & Hall/CRC Press Boca Raton.
39. Liao SJ (2012) Homotopy analysis method in nonlinear differential equations. Higher Edu Press Beijing and Springer-Verlag Berlin Heidelberg.
40. Liu YP, Liao SJ, Li ZB (2013) Symbolic computation of strongly nonlinear periodic oscillations. J Symb Comput 55: 72–95.
41. Abbasbandy S, Hashemi MS, Hashim I (2013) On convergence of homotopy analysis method and its application to fractional integro-differential equations. Quaestiones Mathematicae 36: 93–105.
42. Zheng L, Niu J, Zhang X, Gao Y (2012) MHD flow and heat transfer over a porous shrinking surface with velocity slip and temperature jump Math Comput Modell56: 133-144.
43. Rashidi MM, Kavyani N, Abelman S (2014) Investigation of entropy generation in MHD and slip flow over a rotating porous disk with variable properties. Int J Heat Mass Transf 70 : 892-917.
44. Turkyilmazoglu M (2012) Solution of Thomas-Fermi equation with a convergent approach, Commun. Nonlinear Sci Numer Simulat 17: 4097-4103.
45. Hayat T, Shehzad SA, Ashraf MB, Alsaedi A (2013) Magnetohydrodynamic mixed convection flow of thixotropic fluid with thermophoresis and Joule heating. J Therm Phys Heat Transf 27: 733-740.
46. Schlichting H (1964) Boundary layer theory 6th ed New YorkMcGraw-Hill.